Relative Optical Absorption of Metallic and Semiconducting Single-Walled Carbon Nanotubes

Houjin Huang,* Hisashi Kajiura, Ryuichiro Maruyama, Koji Kadono, and Kazuhiro Noda

Materials Laboratories, Sony Corporation, Atsugi Tec. No. 2, 4-16-1 Okata Atsugi, Kanagawa 243-0021, Japan

Received: August 26, 2005; In Final Form: October 25, 2005

While it is well-known that tube−tube interaction causes changes (peak red-shift and suppression) in the optical absorption of single-walled carbon nanotubes (SWNTs), we found in this work that, upon bundling, the optical absorption of metallic SWNTs (M_{11}) is less affected compared to their semiconducting counterparts (S_{11} or S_{22}), resulting in enhanced absorbance ratio of metallic and semiconducting SWNTs (A_M/A_S). Annealing of the SWNTs increases this ratio due to the intensified tube−tube interaction. We have also found that the interaction between SWNTs and the surfactant Triton X-405 has a similar effect. The evaluation of SWNT separation by types (metallic or semiconducting) based on the optical absorption should take these effects into account.

Introduction

Owing to their exceptional electrical, thermal, and mechanical properties, single-walled carbon nanotubes (SWNTs) have been envisioned as one of the best candidates for many potential applications.[1−3] However, their practical applications, particularly in semiconductor electronics, often require pure carbon nanotubes of the same tube chirality. As current production processes cannot produce carbon nanotubes with a specific chirality, the separation of semiconducting carbon nanotubes from their metallic counterparts has been recognized as one of the critical steps toward nanotube electronic devices. Although some recent progress on the carbon nanotube separation has been reported,[4−10] the lack of an efficient and accurate evaluation method has hampered the further effort in nanotube separation.

Raman scattering has been widely used as a rapid and sensitive evaluation method to monitor the nanotube separation process.[4−7] Because Raman scattering can reveal only tubes with their electronic resonances being matched by the exciting laser, it is difficult to deduce a sample's composition without the use of continuous laser beams with a wide range of wavelengths and a well-controlled sample to avoid any artificial alteration of the resonances.[4] Recently, Strano et al. found that the bundling of SWNTs could cause a significant change in the Raman scattering spectrum, particularly in the radial breathing mode (RBM) region.[13] This finding caused serious concerns on the previous work involving the use of Raman scattering, without considering the bundling effect, for evaluating the separation of metallic and semiconducting SWNTs.

Optical absorption is another evaluation method that has also been widely used for monitoring the nanotube separation process and even for quantifying the separated SWNTs.[8−12] While the quantitative nature of the optical absorption method is well-known, its validity for an accurate evaluation of samples having a strong tendency to aggregate, such as SWNTs, needs to be reconsidered In the present work, we found that the relative optical absorbance of metallic to semiconducting SWNTs changes significantly upon bundling and that annealing of the carbon nanotubes intensifies the tube−tube interaction to induce further change in the optical absorbance ratio. Furthermore, the interaction between carbon nanotube and surfactant was demonstrated to cause the similar effect. These observations indicate that quantification of the bulk separation of SWNTs by the optical absorption method is possible, but only after careful elimination of these artificial effects.

Experimental Section

Sample Preparation. Two sources of single-walled carbon nanotubes with different diameter distributions were used in this study. They are HiPco SWNTs ($d \sim 1 \pm 0.3$ nm) and SWeNT SWNTs (also known as CoMoCat SWNTs, Norman, OK), purchased from Carbon Nanotechnologies Inc. (CNI, Houston, Texas) and Southwest Nanotechnologies ($d \sim 0.8 \pm 0.1$ nm), respectively. Both SWNTs were supplied in purified forms with purity >95%. To obtain SWNTs with different bundling size, the commercial samples (~2 mg) were dispersed in pure water (200 mL) with the addition of 1 or 5% Triton X-405 (Aldrich) under bath ultrasonication for 2−5 h, followed by centrifugation at 60 000 g for 0.5−20 h. Both supernatant and precipitate were collected. The precipitate was further re-dispersed in pure water and centrifuged at 10 000 g for 1 h, followed by collecting once again the precipitate of SWNTs bundles.

Characterization. Both scanning electron microscopy (SEM, JEOL JSM-6700F) and atomic force microscopy (AFM, Digital Instruments NanoScope IV/Dimension3100) were used for the evaluation of the bundling state of the nanotubes. AFM at tapping mode was performed on the nanotubes deposited on freshly cleaved mica surface and washed thoroughly with water and ethanol. UV−Vis−NIR (Hitachi U4000) spectra of SWNTs were collected for carbon nanotubes deposited on quartz plates or in surfactant-assisted aqueous suspension. For HiPco SWNTs, the optical absorption peaks around 550 nm (M_{11}) and 730 nm (S_{22}) were used to represent the optical absorbance of metallic and semiconducting SWNTs because of their relative high absorbance and less overlapping with other CNT absorption peaks. For SWeNT SWNTs, the supernatants after centrifugation at different times were used for this study. The relatively isolated

* Corresponding author. E-mail: houjinhuang@yahoo.co.uk. Current address: Department of Chemical and Materials Engineering, University of Dayton, OH 45469. Telephone: 937-229-2666. Fax: 937-229-3433.

10.1021/jp054839i CCC: $33.50
Published on Web 02/18/2006

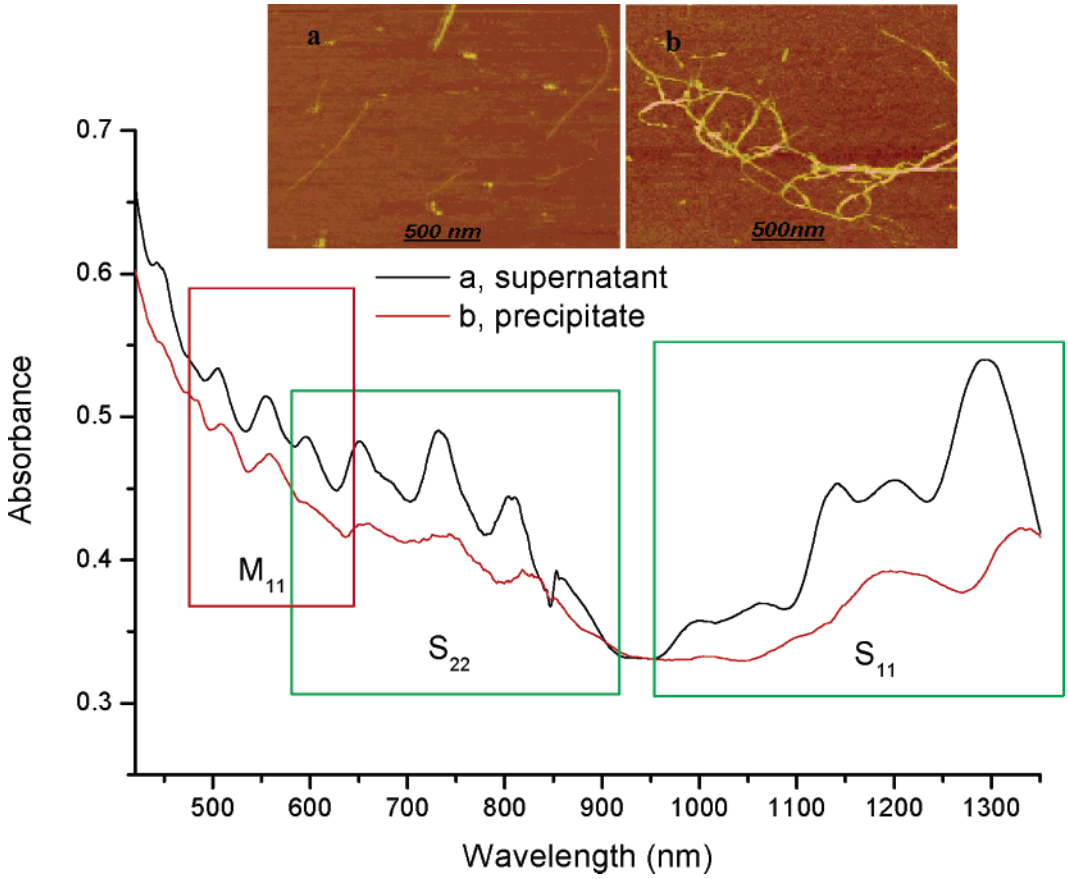

Figure 1. Absorption spectra of HiPco SWNTs in the supernatant (a, black) and the precipitate (b, red), respectively. Both samples are suspended in water by using 1 wt % Triton X-405. The optical absorptions for metallic (M_{11}) and semiconducting (S_{11} and S_{22}) SWNTs are indicated in red and green frames, respectively. The abrupt change in the absorbance around 850 nm is due to instrumental detector switching. The insets show AFM images for the SWNTs from the supernatant (a) and the precipitate (b).

peaks around 450 nm (M_{11}) and 990 nm (S_{11}) were used for comparing their relative absorbance. The above peak assignments were from the literature[11,14] and were further confirmed by our selective reactions of metallic tubes by following Strano's method.[15] Because these peaks comprise several highly overlapped subcomponents and further overlapped over a nonlinear background, it is difficult to distinguish each component by peak fitting, and thus the "peak area" of each selected peak was simply measured after subtracting the linear background between two concave points and used for subsequent analyses. It is important to point out that the use of the peak area does not affect our evaluation on the change of the relative optical absorbance of metallic and semiconducting SWNTs, although the measured "peak area" does not represent its exact absorbance. This is because the measurements for each of the peak areas were done under identical conditions, and only a relative value was concerned. We also noticed that there were some changes in the absorption spectrum for the samples after being stored in ambient atmosphere for a long time (>1 month), due possibly to aggregation and/or air oxidation. Therefore, all the measurements were done with freshly prepared samples, and the results were obtained from statistical analyses of at least six measurements for each of the data points.

Results and Discussion

Figure 1 shows UV−Vis−NIR spectra for both supernatant and precipitate of HiPco SWNTs suspended in water. The absorption peaks of the precipitate are about 5−50 nm, red-shifted compared to that of the supernatant. The red-shift is apparently due to the bundling effect because the carbon tubes in the supernatant are essentially isolated to each other, while the tubes in precipitate are in large bundles (>10 nm), as revealed from AFM images shown in the insets. It appears that the red-shift depends on energy gaps of the SWNTs; the larger energy gap SWNTs correspond to the slighter shifts of the absorption peaks. Detailed description of the relationship between the energy gap and the peak shift will be presented by using SWNTs with fewer tube species, i.e., CoMoCat SWNTs.

While the intensities of the optical absorption for both metallic and semiconducting SWNTs are suppressed upon the intertube interaction, the suppression rates are apparently different for metallic and semiconducting SWNTs. As can be seen from the optical absorption spectra shown in Figure 1, metallic tube peaks around 550 nm are not affected as much as that of their semiconducting counterparts (>650 nm). It also appears that the suppression rates depend on energy gaps of the SWNTs; the larger of the energy gap, the less suppression of the absorption peaks. Shown in parts a and b of Figure 2 are the background-subtracted absorption peaks, representing the electronic transition between the first van Hove singularities of metallic SWNTs (M_{11}) and the electronic transition between the second van Hove singularities of semiconducting SWNTs (S_{22}), respectively. It can be seen that the absorbance decreases by ~16% for M_{11}, while it decreases by ~55% for S_{22}. The absorbance ratio of M_{11} over S_{22} thus increases from 0.33 to 0.63, an enhancement of ~91%. Without considering the bundling effect, one may argue that metallic carbon nanotubes are largely enriched in the precipitate. This is in contrast with our proposition that the bundling effect, instead of the difference

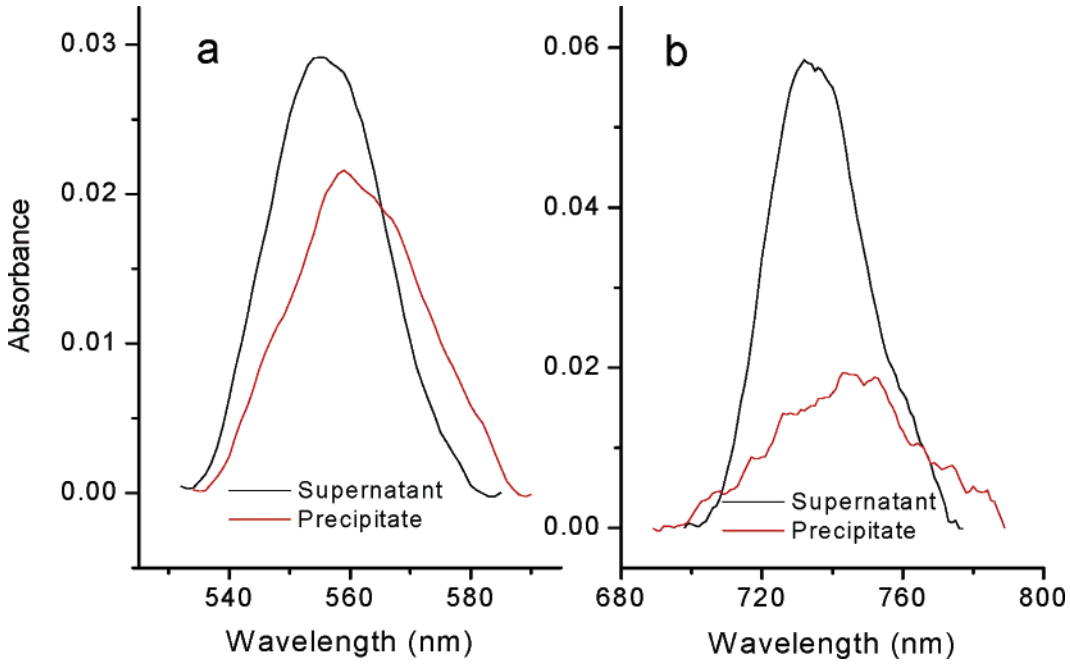

Figure 2. Background-subtracted absorption peaks for metallic (a, M_{11}) and semiconducting (b, S_{22}) HiPco SWNTs remaining in the supernatant (black) and the precipitate (red). The spectra are derived from Figure 1.

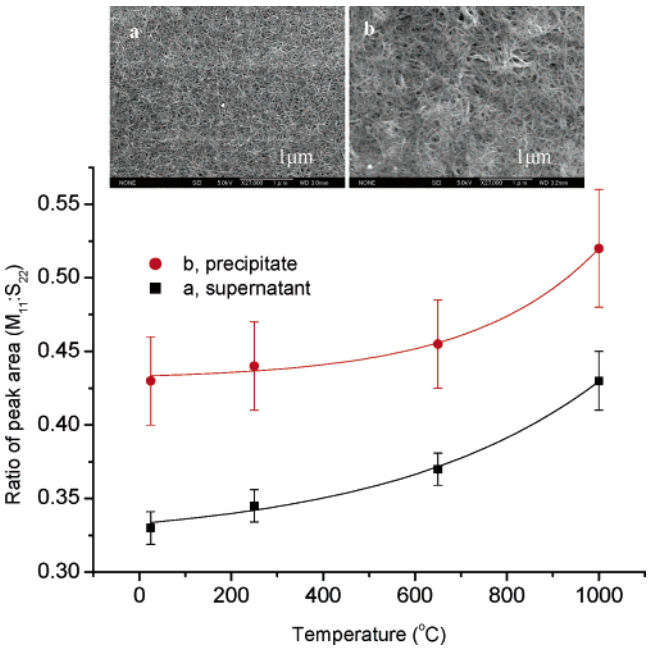

Figure 3. Peak area ratio (M_{11}:S_{22}) for HiPco SWNTs from the supernatant (black) and the precipitate (red) vs annealing temperature. The absorption spectra are taken from SWNTs deposited on quartz plates. The error bars are from different nanotube locations. The guiding lines are fitting results using a function of exponential growth.

in tube composition, induces the enhancement of the absorbance ratio between metallic and semiconducting SWNTs.

To further clarify the influence of the tube−tube interaction on the absorbance ratio between metallic and semiconducting SWNTs, we deposited the supernatant and the precipitate on quartz plates to form CNT thin films and then annealed the films at different temperatures. The result is shown in Figure 3. Two apparent features can be seen in this figure. First, the peak area ratios ($A_{M_{11}}$:$A_{S_{22}}$) for the thin film formed from the precipitate are generally 20−30% higher than that for the supernatant after annealing at the same temperature, while the difference between the ratios decreases gradually along with the increase of the annealing temperature. Second, for the CNT film of both precipitate and supernatant, the peak area ratio ($A_{M_{11}}$:$A_{S_{22}}$) increases along with the annealing temperature, but in a nonlinear behavior.

Higher peak area ratio ($A_{M_{11}}$:$A_{S_{22}}$) for SWNT thin film from the precipitate compared to that from the supernatant can also be understood from their different bundling states, as shown in the inserted SEM images in Figure 3. While it is difficult to deduce the bundle size distributions due to the electron charging effect and highly curved nature of the SWNT bundles, the bundle sizes of SWNTs from the supernatant are generally less than 5 nm, while that from the precipitate are much larger (>20 nm). The larger the bundle size, the larger the tube−tube interaction area averaged to each tube, and thus the stronger the bundling effect on the optical absorption.

It is believed that annealing can remove impurities and functional groups, such as −COOH, from the carbon nanotube surface, and hence enhance the tube−tube interactions. A higher annealing temperature leads to a more effective clean up process, and hence a stronger tube−tube interaction. The increase of the relative optical absorbance of metallic over semiconducting SWNTs along with the annealing temperature further support our proposition that tube−tube interaction affects more the optical absorption of the second van Hove transition of semiconducting SWNTs (S_{22}) than the first van Hove transition of metallic (M_{11}) SWNTs.

The bundling effect on the optical absorption of metallic and semiconducting SWNTs can be more clearly seen in SWeNT SWNTs because of their simpler absorption spectrum compared to that of HiPco SWNTs. Figure 4a shows optical absorption spectra of the nanotubes suspended in water after centrifuging for 0.5 h (red) and 20 h (black) at 50 000 g, respectively. AFM images of the carbon nanotubes on mica show that the suspension after 20 h of centrifuging is almost free of bundles, while the majority of SWNTs in suspension after 0.5 h of centrifuging is still in bundles. Correspondingly, the absorption peaks for the suspension after 0.5 h of centrifuging are red-shifted compared to that after 20 h of centrifuging. It is also notable that the extent of the red-shifts depends on the absorption

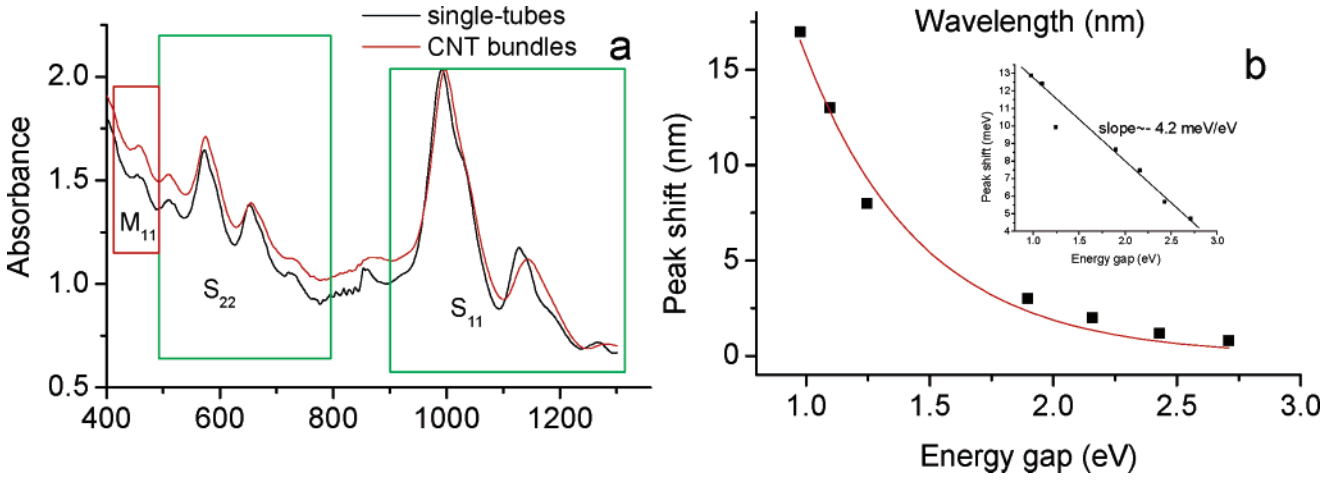

Figure 4. (a) Absorption spectra of SWeNT SWNTs suspended in water with ~1 wt % Triton X-405 after centrifugation for 0.5 h (red) and 20 h (black) at 50 000 g. (b) Peak red-shift in wavelength vs energy gap in eV, corresponding to the peak position. The solid line is a fitting result, using a function of exponential decay. The inset shows peak shift in meV vs energy gap in eV.

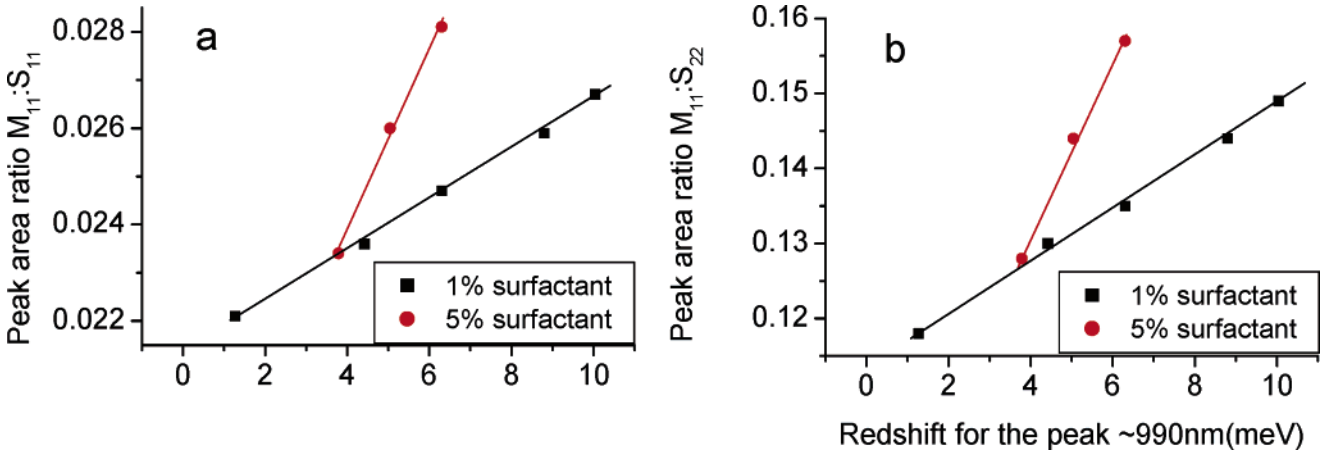

Figure 5. Peak area ratios (a, M_{11}:S_{11} and b, M_{11}:S_{22}) vs absorption peak shift around 990 nm for SWeNT SWNTs suspended in water with addition of 1 wt % (black) or 5 wt % (red) Triton X-405. The data are collected from nanotube suspension centrifuged at a different time period at 50 000 g. The peaks around 450 nm, 572 nm, and 990 nm are used to represent M_{11}, S_{22}, and S_{11}, respectively. The straight lines are guides to the eye.

peak position: the smaller the absorption energy gap, the larger the shift. For example, upon bundling, the peak around 1130 nm (0.97 eV) shifts red by 15 nm, while the peak around 570 nm (2.16 eV) shifts red by only 1.9 nm. The peak shift in wavelength exponentially decays with the absorption energy gap in eV, as shown in Figure 4b. Further analysis of the data indicates that the peak shift in energy is inversely proportional to the energy gap (eV) with a slope of about −4.2meV/eV, as shown in the inset of Figure 4b. This clearly supports that the optical absorption of metallic SWNTs (M_{11}) is less affected by intertube interaction compared to that of semiconducting SWNTs (S_{11} and S_{22}).

Parts a and b of Figure 5 show peak area ratios of M_{11}:S_{11} and M_{11}:S_{22} vs the red-shift of the peak around 990 nm, respectively. Because the absorption peak shift is closely related to the bundling state of SWNTs, we can also use the peak positions to compare the relative bundling state of SWNTs. For SWeNT SWNTs, the peak around 990 nm was chosen for this purpose due to its high intensity. It can be seen that both of the peak area ratios, $A_{M_{11}}$:$A_{S_{11}}$ and $A_{M_{11}}$:$A_{S_{22}}$, increase linearly with the peak red-shift value. That is to say, the peak area ratios increase with the bundling level of the SWNTs, which is in consistent with the trend observed in HiPco SWNTs.

In addition, we found that the interaction between surfactant and carbon nanotubes can also enhance the peak area ratios. For example, the peak area ratio $A_{M_{11}}$:$A_{S_{11}}$ increases by about 15% when the percentage of the surfactant Triton X-405 is increased from 1 to 5 wt % for the suspension, with the major S_{11} peak appearing at 996 nm. The peak area ratios vs peak red-shifts for different percentages of the surfactant are also shown in Figure 5. It can be seen that the higher the percentage of the surfactant, the higher the sensitivity of the peak area ratios over the peak red-shifts.

The underlying mechanism for the above tube-type and band gap-dependent bundling and surfactant effects is not well understood. A simple electrodynamics model may give a brief explanation. Compared to electron transition of S_{11} in semiconducting carbon tubes, the electron transition of M_{11} in metallic nanotubes may be better shielded from the surroundings due to its Fermi electron screening effect. For semiconducting SWNTs, the electrons in outer shell S_{11} may shield the inner electrons in S_{22}, and thus S_{22} is less affected than S_{11}. Because the singularity gap of M_{11} is larger than that of S_{22}, the electron screening effect may be more prominent for M_{11} due to both its deeper electronic level and Fermi electron screening effect.

In summary, we have demonstrated in this work that the optical absorption of metallic and semiconducting SWNTs could be largely affected by their surrounding compositions. The interactions with other tubes, even with the surfactant used for dispersion, can significantly enhance the optical absorbance ratio

of metallic over semiconducting SWNTs due to their different electronic structures. Annealing of the SWNTs increases this ratio due to the intensified tube−tube interaction. A simple electrodynamics model was proposed to explain the phenomena. Evaluation of the separation of metallic and semiconducting SWNTs based on optical absorption spectroscopy should take these influences into account.

References and Notes

(1) Saito R.; Dresselhaus, G.; Dresselhaus, M. S. *Physical Properties of Carbon Nanotubes*; Imperial College Press: London, 1998.

(2) Tans, S. J.; Verschueren, A. R. M.; Dekker, C. *Nature* **1998**, *393*, 49.

(3) Dürkop T.; Getty S. A.; Cobas E.; Fuhrer M. S. *Nano Lett.* **2004**, *4*, 35.

(4) Weisman R. B. *Nat. Mater.* **2003**, *2*, 569.

(5) Banerjee S.; Hemraj-Benny T.; Wong S. *J. Nanosci. Nanotechnol.* **2005**, *5*, 841.

(6) Krupke, R.; Hennrich, F.; von Lohneysen H.; Kappes, M. M. *Science* **2003**, *301*, 344.

(7) Chattopadhyay, D.; Galeska, L.; Papadimitrakopoulos, F. *J. Am. Chem. Soc.* **2003**, *125*, 3370−3371.

(8) Chen, Z.; Du, X.; Du, M.; Rancken, C. D.; Cheng, H.; Rinzler, A. G. *Nano Lett.* **2003**, *3*, 1245−1249.

(9) Zheng, M.; Jagota, A.; Strano, M. S.; Santos, A. P.; Barone, P.; Grace Chou, S.; Diner, B. A.; Dresselhaus, M. S.; Mclean, R. S.; Bibiana Onoa, G.; Samsonidze, G. G.; Semke, E. D.; Usrey, M.; Walls, D. J. *Science* **2003**, *302*, 1545.

(10) Zheng, M.; Jagota, A.; Semke, E. D.; Diner, B. A.; McClean, R. S.; Lustig, S. R.; Richardson, R. E.; Tassi, N. G. *Nat. Mater.* **2003**, *2*, 338−342.

(11) An, K. H.; Park, J. S.; Yang, C.-M.; Jeong, S. Y.; Lim, S. C.; Kang, C.; Son, J.-H.; Jeong, M. S.; Lee, Y. H. *J. Am. Chem. Soc.* **2005**, *127*, 5196.

(12) Maeda, Y.; Kimura, S. I.; Kanda, M.; Hirashima, Y.; Hasegawa, T.; Wakahara, T.; Lian, Y.; Nakahodo, T.; Tsuchiya, T.; Akasaka, T.; Lu, J.; Zhang, X.; Gao, Y.; Yu, Y.; Nagase, S.; Kazaoui, S.; Minami, N.; Shimizu, T.; Tokumoto, H.; Saito, R. *J. Am. Chem. Soc.* **2005**, *127*, 10287.

(13) Heller, D. A.; Barone, P. W.; Swanson, J. P.; Mayrhofer, R. M.; Strano, M. S. *J. Phys. Chem. B* **2004**, *108*, 6905.

(14) Zheng, M.; Diner, B. A. *J. Am. Chem. Soc.* **2004**, *126*, 15490.

(15) Strano, M. S.; Dyke, C. A.; Usrey, M. L.; Barone, P. W.; Allen, M. J.; Shan, H.; Kittrell, C.; Hauge, R. H.; Tour, J. M.; Smalley, R. E. *Science* **2003**, *301*, 1519.